# Wireless Tactile Sensing Element Using Stress-Sensitive Resonator

Hiroyuki Shinoda and Hideki Oasa

***Abstract*—Robots that work with humans require a soft sensor skin to cover the entire body. In this paper, we propose a new method to realize such a skin. By implanting wireless sensing elements in an elastic body, we obtain an elastic and tough sensor skin which is able to be shaped freely. The element is a passive resonator chip whose resonant frequency reflects the stress around the chip. The resonant frequency is read out by a ground coil located at the bottom of the skin. The chip is simply composed of three functional parts, a coil for receiving and transmitting electrical power with wireless coupling, capacitance sensitive to stress, and ceramic resonator to provide high-*Q* resonance. The high quality factor brought by the ceramic resonator enables us to distinguish a large number of chips, and to sense the stress with high accuracy. The structure, the method of wireless signal detection, and basic experiments of tactile sensing are presented.**

***Index Terms*—Haptic interface, resonance measurement, robot sensor, sensitive skin, tactile sensor, telemetry, wireless sensing.**

## I. Introduction

As WAS summarized in [1], many types of tactile sensing devices have been proposed so far. Although large numbers of studies were reported, especially in the last ten years, the tactile sensation has not been utilized effectively in mechatronics system. As stated in [1], one of the reasons is that we have not fully understood what physical parameters we should sense and how we should extract tactile information from them. The other reason is the difficulty of fabricating the device which must be elastic and whose tactile sense must be distributed over a wide area of skin, unlike a localized sensory organ of sight or hearing. Recently, some new technological fields are showing the need for practical artificial tactile sensing. One important need is a sensor skin covering the entire body of robots to work with humans safely. For this purpose, the previous tactile sensing methods lack one or more of the following: elasticity, mechanical toughness, and practical simplicity of fabrication. In a pioneering work of an entire body perception, an interesting idea of a sensing suit [2] was proposed. The sensing fabric is more flexible than a film-type sensor [3] which can be rolled but cannot extend, but the instability of electrical contact among strings is difficult to avoid. Polymer electronics [4] are a hope, but they are not yet at a practical level. From past methods, we find that these defects come from the wiring. If we can place small sensing elements in an elastic body without wiring, the skin will be tough and elastic, as well as easy to fabricate in a free shape. Based on this consideration, we recently proposed a method called "telemetric skin" [5]. By implanting small sensing chips which can receive electrical power and transmit tactile signals by inductive coupling without wiring, we could easily obtain elastic free-shaped sensory skin. In that research, the signal was produced by an integrated circuit on the sensing chip. Therefore, it had the merit of easiness of development into a multifunctional sensing chip. Meantime, we are afraid the cost might be too high for practical use, especially at the early stage. In this paper, we propose a new wireless tactile sensing device. Signal transmission based on inductive coupling between sensing chips and a ground coil is the same as the former telemetric skin. The new component is that the sensing chip is composed of only passive components without transistors. Therefore, the energy consumption for sensing is much smaller than the former telemetric skin needing the minimum inductive voltage to activate the silicon semiconductor circuit; nevertheless, each chip gives a highly accurate digital signal representing the pressure around the chip.

In recent years, some methods of wireless signal transmission from remote sensors without a battery [6]–[9], have been proposed. After exciting the remote sensor device consisting of passive parts by interrogation RF signal, they observe the energy released which contains information. Here, we give a new principle to miniaturize them into a large number of small tactile elements in a skin. We show the structure of the sensing system, and a method to read out sensor signals with high resolution in noise. We examined the theory in basic experiments with prototype sensing chips.

## II. Available Physical Phenomenon for Wireless Tactile Sensing

The basic concept of wireless tactile sensing is shown in Figs. 1 and 2. If we have a resonator which has some electromagnetic interaction with the ground coil located at the bottom of the skin, and whose resonant frequencies are sensitive to the stress around it, the resonator can be a wireless tactile sensing chip. A simple $LC$ resonator, as shown in Fig. 2, whose capacitance is stress sensitive and whose coil is inductively coupled with the ground coil, is an example of it. The shift of the resonant frequency that reflects the stress is obtained wirelessly, by inductive excitation and observation of the relaxation with a ground coil. We obtain a stress distribution by detecting resonant frequencies of multiple chips sequentially. The technique to assign a resonant frequency to each tactile element as an index is seen in [10].

Manuscript received March 1, 2000; revised June 21, 2000. Recommended by Guest Editors M. Kaneko and R. C. Luo. This work was supported in part by the Japan Society for the Promotion of Science under Grant JSPS-RFTF 96P00801.

The authors are with the Faculty of Engineering, Tokyo University of Agriculture and Technology, Tokyo 184-8588, Japan (e-mail: shino@cc.tuat.ac.jp).

Publisher Item Identifier S 1083-4435(00)07826-1.

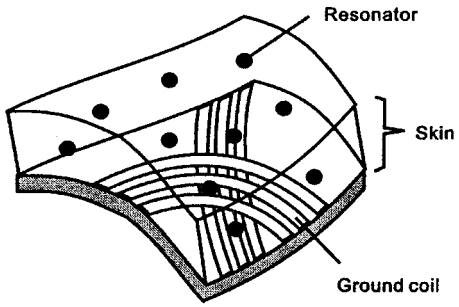


Fig. 1. Basic concept of wireless tactile sensing.

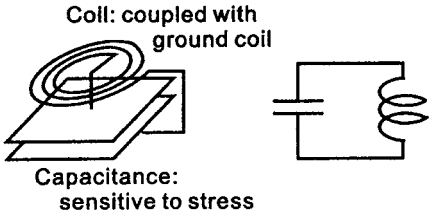


Fig. 2. A simple example of tactile resonator to explain the concept of wireless tactile sensing.

A desirable resonator has high accuracy, quick response, and low crosstalk with other resonators having close resonant frequencies. For obtaining high accuracy and low crosstalk, the resonator must have high $Q$ (quality factor). In order to obtain quick response without losing the accuracy and the low crosstalk, the resonant frequency must be as high as possible. Therefore, a simple $LC$ resonator is not proper for this tactile chip because the $Q$ is less than 100 at frequencies higher than, for example, 1 MHz.

Other than $LC$ resonance, several resonant phenomena are known. One is acoustic resonance. Resonance of quartz has both very high $Q$ ($\sim 10^5$) and high resonant frequency. Ceramic resonators also have high $Q$ (over $10^3$). A surface acoustic wave (SAW) device can have high $Q$ factor up to $10^4$, and the resonant frequency and quality factor are controllable by patterning of a two-dimensional electrode [8]. Another interesting resonance is nuclear magnetic resonance (NMR). The high quality factor and the coupling with electromagnetic field enables minute and noninvasive human body imaging, as well as analysis of material property. The difficulty of applying an NMR signal to tactile sensing is that the signal is weak, and that it needs a strong magnetic field [11].

## III. Structure of Sensing Chip

In this paper, we propose a sensing resonator as shown in Fig. 3. The chip is composed of three functional parts, a coil $L$ for receiving and transmitting electrical power, capacitance $C$ which is sensitive to stress, and ceramic resonator $X_C$ to provide high-$Q$ resonance. The radial cut of the sensing capacitor is for preventing induction current which interferes with the coupling between the chip coil and the ground coil. The fabrication process of these parts has been well established. It is already possible to make the coil and the sensing capacitor

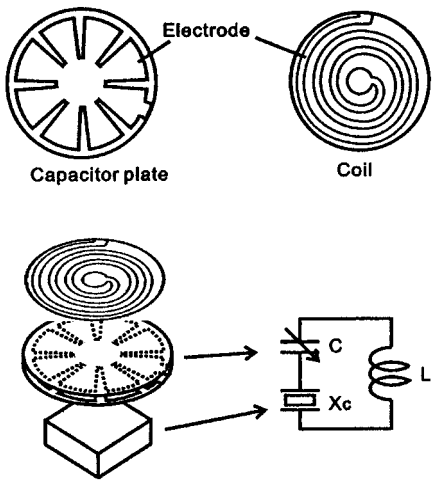


Fig. 3. The sensing resonator proposed here. The chip is composed of three functional parts, a coil for receiving and transmitting electrical power, capacitance which is sensitive to stress, and ceramic resonator to provide high-$Q$ resonance. The radial cut of the sensing capacitor is for preventing induction current which interferes the coupling between the chip coil and the ground coil.

on a single silicon chip. The $C$ reflects the following stress around the chip:

$$A\sigma_{zz} + B(\sigma_{xx} + \sigma_{yy}) \tag{1}$$

where $\sigma_{zz}$ is the normal stress vertical to the chip, and $\sigma_{xx}$ and $\sigma_{yy}$ are two normal stress components parallel to the chip surface. The ratio of the constants $A$ and $B$ is determined by the thickness and the width of the chip [12], and it is also sensitive to shear stress for large deformation.

A sensing chip based on an SAW device [8] instead of $C$ and $X_C$ will be another challenging method. It is attractive in that we can use not only frequency but also signal delay to distinguish a large number of chips [6]. However, we have to increase the operating frequency over 1 GHz to make the chip size smaller than several millimeters. Therefore, we examine another sensing chip using $C$ and $X_C$, as shown in Fig. 3.

The equivalent circuit of the ceramic resonator is illustrated in Fig. 4(a). The ceramic resonator has both a zero and a pole. The reactance of the serial connection of $L$, $C$, and $X_C$ is shown in Fig. 4(b) and (c). The resonant frequency to maximize the circuit current in Fig. 3 is the frequency at which the following reactance:

$$X = X_C + \omega L + \frac{1}{\omega C} \tag{2}$$

becomes zero. In a simple $LC$ resonator, the large resistance contained in $L$ results in a low quality factor. However, in this $L$–$C$–$X_C$ resonator, the equivalent inductance $L_0$ in $X_C$ can be much larger than $L$, which brings higher quality factor than that of the simple $LC$.

Sensing is done by $C$. We can calculate the sensitivity, neglecting $\omega L$, as

$$\frac{\Delta F_r}{F_r} = -\left(\frac{1}{1 + C_1/C} \cdot \frac{1}{1 + (C + C_1)/C_0}\right)\frac{\Delta C}{C}. \tag{3}$$

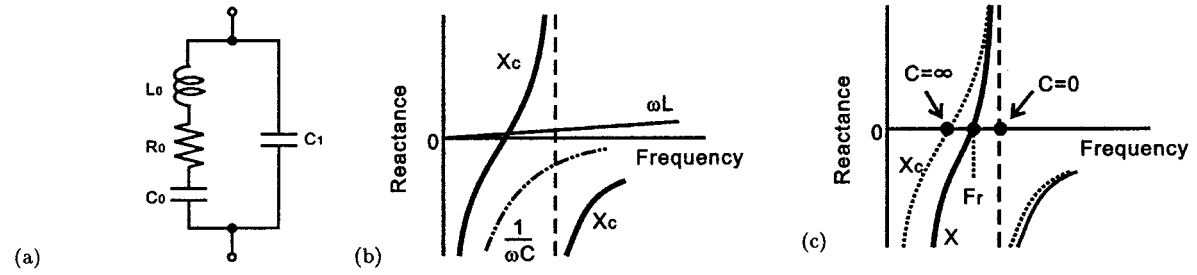


Fig. 4. (a) Equivalent circuit of quartz and ceramic resonator. (b) Illustrating reactance of $L$, $C$, and $X_C$. (c) The reactance $X$ of the serial connection of $L$, $C$, and $X_C$. The resonant frequency $F_r$ is the zero.

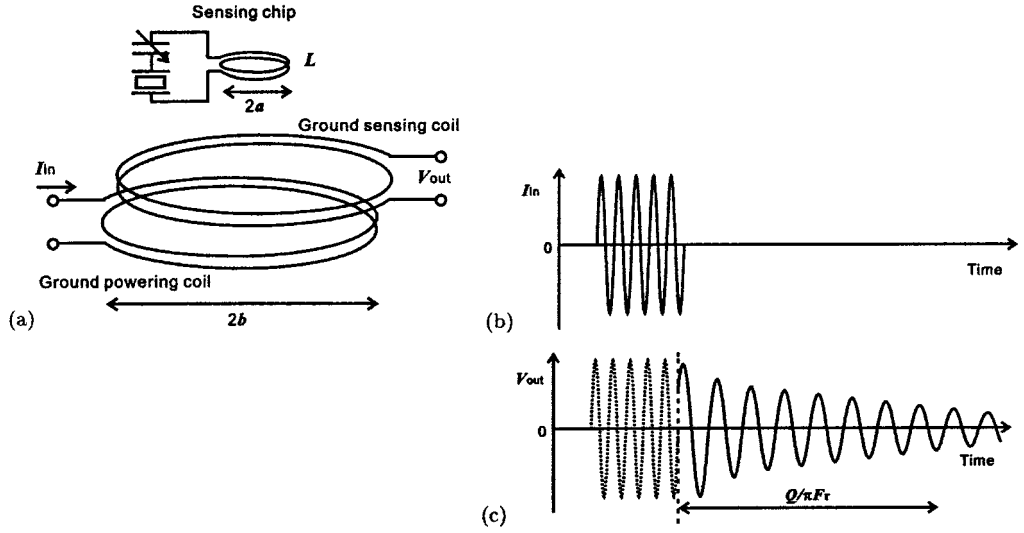


Fig. 5. Schematic diagram of resonant frequency sensing. We observe the output voltage $V_{\rm out}$ for an input burst signal. The output voltage is a decaying signal with the resonant frequency $F_r$ of the sensing chip. The duration of the decay is $Q/F_r$. The output amplitude is maximized when the exciting frequency is equal to $F_r$.

Therefore, if $C$ is comparable to $C_0$ and $C_1$, the frequency change rate is comparable to the change rate of $C$. The resistance of the serial connection of $C$ and $X_C$ at $F_r$ is given as

$$\mathrm{Re}[X(f=F_r)] = \left(1+\frac{C_1}{C}\right)^2 R_0. \tag{4}$$

Thus, the equivalent resistance increases by attaching $C$. This means a smaller $C$ than $C_1$ weakens the signal amplitude. It will be informative to show typical parameters of a commercial resonator. In an 8-MHz resonator (Murata, Ceralock), $L_0 = 68$ $\mu$H, $C_0 = 6.4$ pF, $R_0 = 4.5\ \Omega$, and $C_1 = 39.6$ pF.

## IV. Signal Intensity and Chip Design

A schematic diagram of signal detection is shown in Fig. 5. First, we give the ground coil a burst current $I_{\rm in}$, as shown in Fig. 5(b), to excite a chip. After stopping $I_{\rm in}$, we observe the output voltage of another ground coil driven by the excited resonator. (It is also possible to use only one coil for both excitation and observation.) The frequency of output voltage is always the resonant frequency $F_r$, regardless of the excitation frequency, while the amplitude is maximized when the excitation frequency is equal to $F_r$. The signal decays with time constant $Q/\pi F_r$. As we show in the next section, we measure the frequency of this signal.

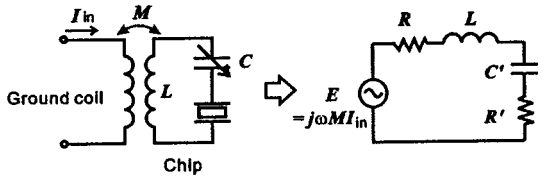


Fig. 6. Equivalent circuit for understanding the resonant current at the chip coil $L$.

Next, we examine the theoretical signal intensity. In Fig. 6, the $R$ is the equivalent resistance contained in the coil $L$ at the resonant frequency. The $C'$ and $R'$ represent the impedance of the serial connection of $C$ and $X_C$ at the resonant frequency. When $L$ is sufficiently small, the $R'$ is approximated as (4).

Assume a chip coil with radius $a$ and turn $n$ is located at the center of the circular ground powering coil which has radius $b$ and turn $n_G$. Then, the mutual inductance $M$ between them is written as

$$M = \mu_0 \frac{\pi a^2}{2b} n_G n \tag{5}$$

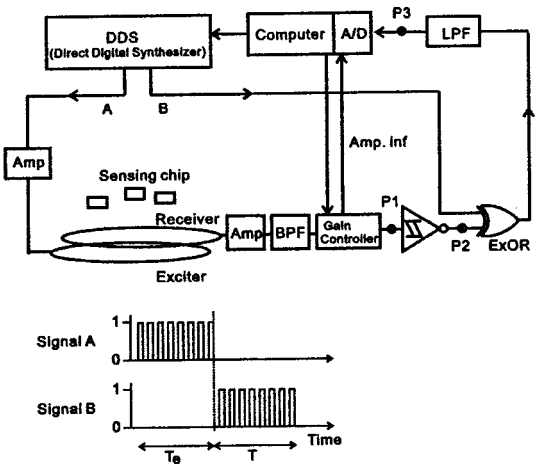


Fig. 7. Block diagram of resonant frequency detection. Signal $A$ excites the chip for $T_e$, and signal $B$ is used for a reference signal.

where $\mu_0$ is the vacuum permeability. Therefore, the observed voltage $V_{\text{out}}$ is given as

$$V_{\text{out}} = \frac{\omega^2 MM'}{R+R'} I_{\text{in}} = \left(\frac{\pi\mu_0}{2b}\right)^2 \frac{\omega^2 a^4 n^2}{R+R'} n_G n'_G I_{\text{in}} \quad (6)$$

where $M'$ is the mutual inductance between the chip coil and the ground sensing coil, and $n'_G$ is the turn of the ground sensing coil.

For example, when $\omega = 10\,\text{MHz} \times 2\pi$, $a = 2$ mm, $b = 5$ cm, $n_G = n'_G = n = 5$, and $R + R' = 10\,\Omega$, (6) is calculated into

$$V_{\text{out}}\ \text{V} = 0.006 I_{\text{in}}\ \text{A}. \quad (7)$$

At a low frequency, (6) tells us that the observed voltage is proportional to the square of the chip-turn $n$ when $R < R'$. However, in our experiments, up to 40 turns at 10 MHz (for chip coil radius 2 mm, by 50-$\mu$m-radius wire), the output voltage did not increase where $n > 10$, because the $R$ increased at a comparable rate [13].

## V. Frequency Detection

Fig. 7 shows the procedure of resonant frequency detection. A digital-based circuit brings easy detection of multimode resonance. After we mold the sensor skin, the computer scans over the total bandwidth of all resonators, for obtaining a rough estimate of each resonant frequency from the peak frequency. Using these recorded initial frequencies, we detect the precise resonant frequencies of chips one by one as follows.

### A. Primitive Method

One primitive method is counting the alternation of relaxation signal. To obtain the highest accuracy, we excite each chip during $T_e \sim Q/F_r$ and observe the relaxation signal during $T \sim Q/F_r$. The frequency error $\Delta F_r$ is given as

$$\frac{\Delta F_r}{F_r} = \frac{1}{TF_r} = \frac{1}{Q}. \quad (8)$$

For example, let $F_r$ and $Q$ be 10 MHz and 1000, respectively. If we assign 0.1-MHz bandwidth, that is, 1% of 10 MHz for each chip, the dynamic range is $10^1$, that is, about 3 bits. One method to improve this is to use a resonator with a higher $Q$. Another one is to widen the bandwidth. However, the former makes the response slow, and the latter makes the maximum number of available sensing chips small.

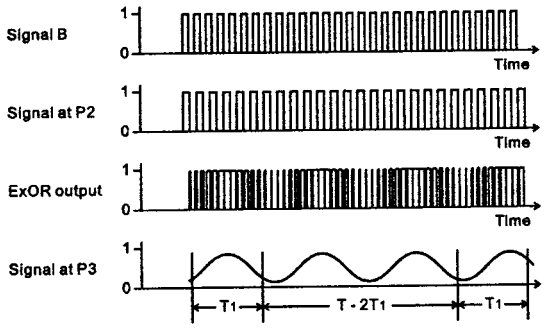


Fig. 8. Illustration of processed signals. The frequency difference between the driving signal (signal $B$) and the detected signal (signal at $P2$) is obtained from the waveform at $P3$.

### B. Method for Higher Resolution

A method to obtain higher frequency resolution is to measure the period of the signal more precisely, as we have *a priori* knowledge that the signal has a single frequency. After shifting the signal frequency to a lower frequency through multiplication with a reference signal, we obtain its period from the waveform, which gives a more precise signal frequency as follows. The block diagram in Fig. 7 shows the procedure. The received signal goes through a bandpass filter (BPF) whose passband covers the total bandwidth of all resonators, and after converting to a 1-bit signal as shown in Fig. 8, we take exclusive-OR with the reference signal. After low-pass filtering, we get the analog waveform $g(t)$ into a computer. The frequency of the waveform $g(t)$ is equal to the difference between the reference signal and the received signal.

The period of $g(t)$ is calculated from zero crossings of a filtered signal $g * \phi(t)$ where $\phi(t)$ is a quasi-Gaussian kernel

$$\phi(t) = \begin{cases} \exp\{-\beta(t/T_1)^2\}\sin(\omega_0 t), & (|t| < T_1) \\ 0, & (|t| > T_1). \end{cases} \quad (9)$$

The parameter $\omega_0$ is a rough estimate of the frequency of $g(t)$, and we choose $\beta = 4.0$ to make the envelope smooth. We obtain the signal period from the zeros of $g * \phi(t)$ in $[T_1, T - T_1]$, excluding both ends of $T_1$ data. As we show in Appendix A, the best estimate is obtained when $T_1 = T/6$.

As Appendix B shows, the accuracy of frequency detection by this method is given as

$$\frac{\Delta F_r}{F_r} = \frac{n_d\sqrt{F_r}}{(TF_r)^{1.5}A} = \frac{N}{(TF_r)^{1.5}A} > \frac{N}{Q^{1.5}A} \quad (10)$$

where $A$ and $n_d$ are the amplitudes of the signal and the noise density at the signal frequency, respectively, at point $P1$ before digital operation in Fig. 7. The $N = n_d\sqrt{F_r}$ is the amplitude of an imaginary noise which is white up to $F_r$ with a noise density $n_d$. If the signal-to-noise ratio (SNR) is 10 dB for a white noise, the resolution is improved 100 times compared with (8), for the same data length $T$.

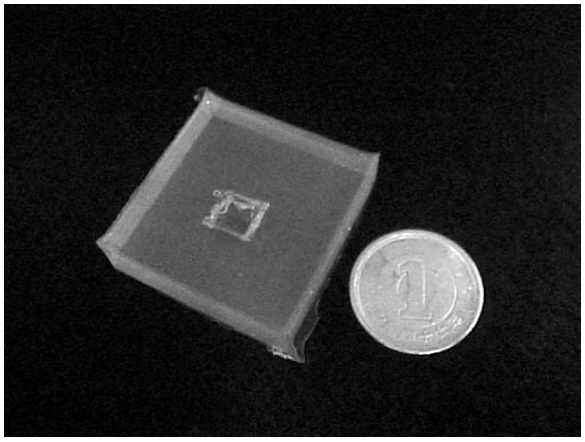

Fig. 9. Prototype of the sensing chip surrounded by a transparent silicone rubber.

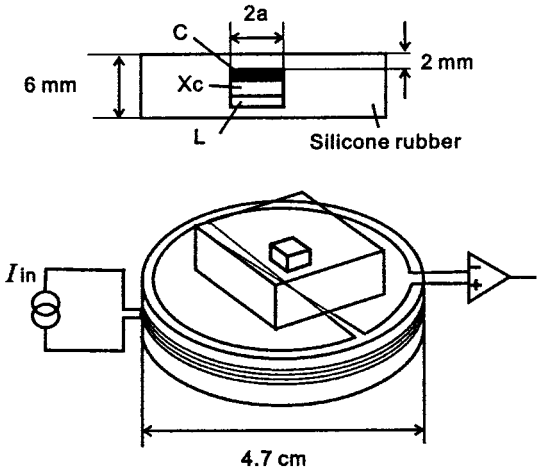


Fig. 10. Experimental setup. We observe the resonant frequency of the sensing chip while we push on the silicon robber surface. The ground powering coil is 4.7 cm in diameter with 50 turns, while the sensing coil is 1 turn, which is twisted to reduce the coupling with the powering coil.

## VI. Experiment

We fabricate two prototypes of sensing chip with silicone rubber molding as shown in Fig. 9, and examine the theory using the experimental setup shown in Fig. 10. One operates at 900 kHz, and the other one is a practical 8-MHz chip. In both chips, the sensing capacitor is made of two copper plates with oxidized surfaces facing each other. Sensitivity to pressure is given by the natural unevenness of the plates. To tune $C$ into a proper capacitance, we attached a chip capacitor parallel to the sensing capacitor. That capacitance is described in Table I as "(+47 pF)." Although the shape of the chip is a circle in Fig. 3 to avoid stress concentration, here, we fabricate the sensing capacitor in a square shape for convenience. The coil $L$ is made of wire 0.1 mm in diameter. The dimension of each part is summarized in Table I. The size of the ceramic resonators described in the table is not that of the resonator itself, but that of the package. Except for $L$, we can miniaturize them without losing sensing ability. In 900-kHz operation, we need many turns for signal intensity, as is shown in the theory, and a low-frequency chip is slow in response. Therefore, it is not practical, however we fabricate it at first for obtaining reference data.

TABLE I
Parameters of Sensing Chips

| | |
|---|---|
| | 900 kHz |
| L | 100 turn, $a = 4.2$ mm |
| C | 15 pF, $7 \times 7 \times 0.5$ mm (+ 47 pF) |
| $X_C$ | 895 kHz, $6 \times 5 \times 2$mm |
| | 8 MHz |
| L | 5 turn, $a = 2.2$ mm |
| C | 13 pF, $5 \times 5 \times 0.5$ mm (+ 10 pF) |
| $X_C$ | 7.98 MHz, $4.5 \times 4 \times 1.6$ mm |

### A. Results of the 900-kHz Chip

Fig. 11(a) shows an output signal with no sensing chip. Only a driving signal is observed. The input current $I_{\rm in}$ is 6 mA in effective value. Fig. 11(b) is a signal by the sensing chip at the resonant frequency. The resonance is observed. Here, the output voltage is amplified 12000×. In this basic experiment, the BPF in Fig. 7 is not inserted. The effective noise value is 0.2 V. The waveform at point $P3$ in Fig. 7 is shown in Fig. 11(c). We estimate the frequency from the data during $T = 512$ $\mu$s with 1-MHz sampling.

The plots in Fig. 12 are the detected frequencies by this procedure. When we pressed the sensor surface using an acrylic resin cylinder with 5-mm radius just over the sensing chip, the resonant frequency changed. Since the rubber thickness was comparable to the pressing depth, the frequency change that is expected to reflect the stress showed nonlinearity to the pressing depth. The standard deviations of the frequency detection are plotted in the identical figure. They were estimated from 100 measurements under identical conditions. These plots show the error is smaller than 20 Hz for 0.5-ms observation. The error ratio

$$\frac{\Delta F_r}{F_r} = 20/900\,000 = 2 \times 10^{-5} \tag{11}$$

corresponds to the calculation of (10) when $F_r T = 450$, and SNR = 20 dB.

### B. Results of 8-MHz Chip

The experimental setup is unchanged from the previous one. Also, in this experiment, the preliminary BPF is not inserted. Fig. 13 shows the detected signal. The input current $I_{\rm in}$ is 1 mA in effective value. The signal intensity of 0.5 V in effective value corresponds to the calculation of (6) when we substitute 12 $\Omega$ for $R + R'$. The effective value of the noise was 0.2 V. When we pressed the sensor surface using an acrylic resin cylinder with 5-mm radius just over the sensing chip, the resonant frequency changed as shown in Fig. 14. The applied force at the 1-mm pressing depth was 600 N. The data length used for determining the frequency was $T = 20$ $\mu$s. The standard deviation was 1 kHz. The error ratio

$$\frac{\Delta F_r}{F_r} = 1\ \text{kHz}/8\ \text{MHz} \sim 1 \times 10^{-4} \tag{12}$$

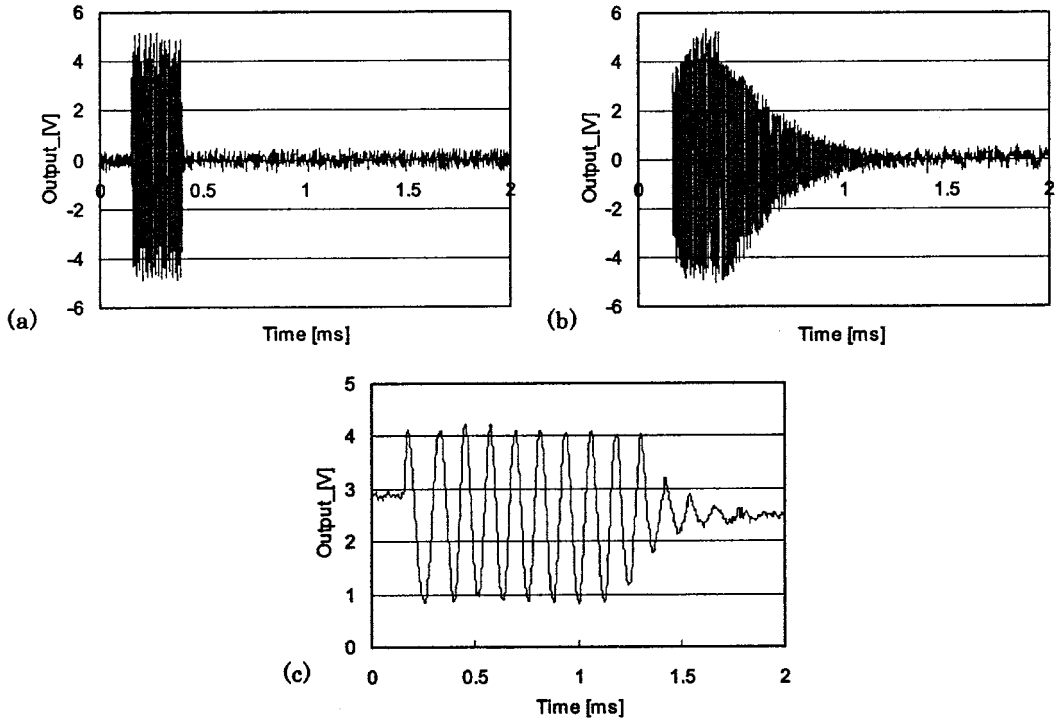


Fig. 11. Experimental results of the 900-kHz chip. (a) ignal $V_{\rm out}$ with no sensing chip at $P1$ in Fig. 7. (b) Resonance signal. (c) Low-passed ExORed signal at $P3$. The driving current is 6 mA.

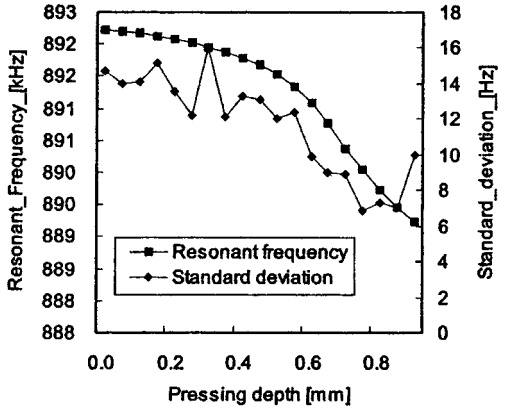


Fig. 12. Experimental results of the 900-kHz chip. Measured resonant frequencies and their errors while we pressed on the sensor surface. The data length used for the frequency estimation is 512 $\mu$s.

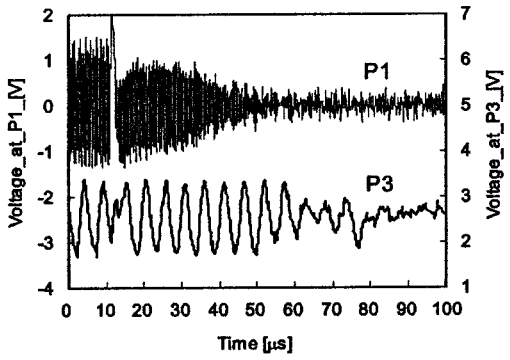


Fig. 13. Experimental results of the 8-MHz chip. Signal $V_{\rm out}$ at point $P1$ in Fig. 7, and the signal at $P3$. The driving current $I_{\rm in}$ was 1 mA.

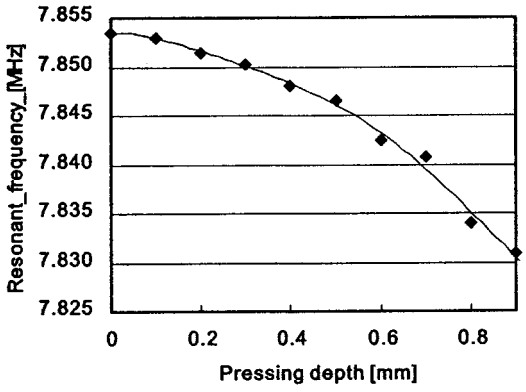


Fig. 14. Experimental results of the 8-MHz chip. Measured resonant frequencies while we pressed the sensor surface. The standard deviation was 1 kHz. The data length used for frequency estimation is 20 $\mu$s.

corresponds to the calculation of (10) when $F_rT = 160$, and SNR $= 10$ dB.

In this experiment, we could obtain a sensing chip whose bandwidth was 30 kHz with 1-kHz resolution. The time needed to get one chip signal was shorter than 100 $\mu$s. In calculation, 100 sensing chips whose initial frequencies span from 10 to 20 MHz with 100-kHz interval take less than 10 ms for all to be measured.

## VII. Summary and Discussion

In this paper, we have proposed a method to realize an elastic sensor skin in a free shape, by implanting wireless passive resonator chips in the skin. We read out the stress on each chip by

a ground coil located at the bottom of the skin. The chip is composed of three functional parts, a coil for receiving and transmitting electrical power with wireless coupling, capacitance sensitive to stress, and ceramic resonator to provide high-$Q$ resonance. First, we showed theories to give signal intensity and sensitivity. Next, we presented a digital-based method to detect the frequency of the resonator chip and the theoretical accuracy. We confirmed the theory with two types of prototype, 900-kHz and 8-MHz resonator chips. As for the 8-MHz chip with radius of 2.2 mm, we could acquire a 5-bit signal within a 30-kHz bandwidth, by 10-$\mu$s observation of a signal with 10-dB SNR.

The theoretical minimum of the chip size is estimated from (6) and the thermal noise. The thermal noise density $v_n$ of the ground sensing coil with a single turn is given as

$$v_n = \sqrt{4k_BTR} \sim 1 \times 10^{-10}\ \mathrm{V}/\sqrt{\mathrm{Hz}} \tag{13}$$

where we assumed the equivalent resistance of the ground coil $R = 0.5\ \Omega$ ($Q \sim 10$) for the radius $b = 1$ cm for a fingertip. If we should detect the signal with 10-dB SNR [$v_n\sqrt{10\ \mathrm{MHz}}/\mathrm{A} = 0.3$, see (10)] as discussed in Section V, (6) gives the minimum radius of the chip coil as

$$a > \frac{10^{1/8}}{\pi}\sqrt{\frac{b}{\mu_0 n}} \cdot \frac{\{(R+R')v_n\}^{1/4}}{F_r^{3/8}(n_G I_{\mathbf{in}})^{1/4}}. \tag{14}$$

If we substitute $n = 5$, $R + R' = 20\ \Omega$, $F_r = 10$ MHz and $n_G I_{\mathbf{in}} = 50$ mA, the minimum of $a$ becomes 0.6 mm. This value of 0.6 mm is not susceptible to the input current, as it is proportional to ${I_{\mathbf{in}}}^{-1/4}$.

Future work includes the practical design of the ground coil and the fabrication of multiple chips. A net-like ground coil proposed for the former telemetric skin [14] will also be applicable to this method. Regarding multiple chip fabrication, few theoretical problems exist. The ceramic resonator chip used in this experiment has frequency stability within $\pm 0.3\%$ over $-20 \sim +80$ °C. Therefore, if we assign 100-kHz bandwidth to a 10-MHz chip with sensing range 40 kHz, no crosstalk happens, which enables 100 chips to operate within the 10 MHz bandwidth. The problem to be solved is the technique to fabricate a large number of resonators which have slightly different initial frequencies.

Endowing the sensing chip with multidimensional sensitivity without losing simplicity is also worth challenging. Usefulness of resolving stress into its components [15], [16] has already been reported.

## APPENDIX A

Since the bandwidth of $\phi$ of (9) is proportional to $1/T_1$, the relative noise amplitude $r$ to the signal amplitude left after $\phi$ filtering is proportional to $1/\sqrt{T_1}$. Then, the error of the signal period estimation is proportional to

$$\frac{r}{T - 2T_1} \propto \frac{1}{TT_1^{1/2} - 2T_1^{3/2}} \tag{15}$$

where $T - 2T_1$ is the data length used for the estimation. This quantity is maximized when $T_1 = T/6$.

## APPENDIX B

Let the signal and the noise at point $P1$ in Fig. 7 be $s(t) = A\cos(2\pi F_r t + \theta)$ and $e(t)$, respectively. For simplicity of description, we omit the BPF and assume the $e(t)$ is a random noise with the bandwidth of $F_r$. It is straightforward to extend this to a general case of noise spectrum. We also express the rectangular signals (without noise) at point $P2$ and after $ExOR$, as $S(t)$ and $S_1(t)$, respectively. The $S(t)$ rises up at $t = t_{2n}$ and drops down at $t = t_{2n+1}$, where $t_n = n/(2F_r)$. Affected by the noise $e(t)$, the inverter's switching time $t_n$ fluctuates randomly into $t_n + \alpha_n$. When the noise amplitude is smaller than $A$, the deviation $\epsilon^2$ of the fluctuation $\alpha_n$ is given as

$$\epsilon^2 = \overline{\alpha_n^2} = \frac{\overline{e(t)^2}}{(ds(t)/dt|_{t=t_n})^2} \sim \frac{\overline{e(t)^2}}{(2\pi F_r A)^2}. \tag{16}$$

If we describe this fluctuated signal $S'(t)$ and its $ExOR$ed signal $S_1'(t)$ as

$$S'(t) = S(t) + E(t) \tag{17}$$

$$S_1'(t) = S_1(t) + E_1(t) \tag{18}$$

where $E(t)$ and $E'(t)$ are functions which take 0, 1, or $-1$, they satisfy

$$|E_1(t)| = |E(t)|. \tag{19}$$

In a low-frequency range $< F_r$, the spectrum of $E(t)$ is identical to that of the following imaginary signal $E'(t)$:

$$E'(t) = \begin{cases} -\alpha_{2n} \cdot 2F_r & (t_{2n} < t < t_{2n+1}) \\ \alpha_{2n+1} \cdot 2F_r & (t_{2n+1} < t < t_{2n+2}) \end{cases}. \tag{20}$$

Because the bandwidth of $E'(t)$ is $F_r$, its power density is

$$p = \frac{\overline{E'(t)^2}}{F_r} = \frac{\overline{(\alpha_n \cdot 2F_r)^2}}{F_r} = 4\epsilon^2 F_r. \tag{21}$$

Since $\alpha_n$ has no correlation with $S(t)$ and $S'(t)$, the power density of $E_1(t)$ at a low frequency is equal to $p$, too.

Next, we express the amplitude of differential frequency component contained in $S_1'(t)$ as $g(t) = B\cos(2\pi Ft + \theta')$, where $B = 4/\pi^2$. Since the bandwidth of the $\phi(t)$ is $W \sim 1/T_1$, the noise amplitude ratio $r$ to the signal, after $\phi$ filtering, is written as

$$r = \frac{\sqrt{p \cdot 1/T_1}}{B} = \frac{\pi^2\epsilon}{2}\sqrt{\frac{F_r}{T_1}}. \tag{22}$$

Now, the estimation error of the period $1/F$ is given as

$$\Delta\left(\frac{1}{F}\right) = \frac{r}{2\pi F} \cdot \frac{1/F}{T - 2T_1}. \tag{23}$$

Combining (16), (22), and (23), using $T_1 = T/6$, we obtain

$$\Delta F_r = \Delta F = \frac{3\sqrt{3}}{8\sqrt{2}} \frac{\sqrt{\overline{e(t)^2}}}{F_r^{0.5} T^{1.5} A}. \tag{24}$$

In (10), the coefficient is omitted.

## REFERENCES


[1] M. H. Lee and H. R. Nicholls, "Tactile sensing for mechatronics—A state of the art survey," *Mechatron.*, vol. 9, no. 1, pp. 1–31, 1999.

[2] M. Inaba, Y. Hoshino, K. Nagasaka, T. Ninomiya, S. Kagami, and H. Inoue, "A full-body tactile sensor suit using electrically conductive fabric and strings," in *Proc. IEEE/RSJ Int. Conf. Intelligent Robots and Systems*, Osaka, Japan, 1996, pp. 450–457.

[3] *F-SCAN System*, Tekscan Inc., South Boston, MA, 1997.

[4] J. D. Madden, S. R. Lafontaine, and I. W. Hunter, "Fabrication by electrodeposition—Building 3D structures and polymer actuators," in *Proc. 6th Int. Symp. Micro Machine and Human Science*, Nagoya, Japan, 1995, pp. 77–81.

[5] M. Hakozaki, H. Oasa, and H. Shinoda, "Telemetric robot skin," in *Proc. 1999 IEEE Int. Conf. Robotics and Automation*, 1999, pp. 957–961.

[6] A. Pohl, "A low-cost high-definition wireless sensor system utilizing intersymbol interference," *IEEE Trans. Ultrason., Ferroelect., Freq. Contr.*, vol. 45, pp. 1355–1362, Sept. 1998.

[7] A. Pohl and L. Reindl, "New passive sensors," in *Proc. 16th IEEE Instrumentation and Measurement Technology Conf.*, vol. 2, 1999, pp. 1251–1255.

[8] A. Pohl, G. Ostermayer, and F. Seifert, "Wireless sensing using oscillator circuits locked to remote high-Q SAW resonators," *IEEE Trans. Ultrason., Ferroelect. Freq. Contr.*, vol. 45, pp. 1161–1168, Sept. 1998.

[9] W. Buff, F. Plath, O. Schmeckebier, M. Rusko, T. Vandahl, H. Luck, F. Moller, and D. C. Malocha, "Remote sensor system using passive SAW sensors," in *Proc. 1994 IEEE Ultrasonics Symp.*, vol. 1, 1994, pp. 585–588.

[10] Y. Yamada, K. Shin, N. Tsuchida, and M. Komai, "A tactile sensor system for universal joint sections of manipulators," *IEEE Trans. Robot. Automat.*, vol. 9, pp. 512–517, Aug. 1993.

[11] A. U. Rahman, *Nuclear Magnetic Resonance—Basic Principles*. New York: Springer-Verlag, 1986.

[12] H. Shinoda, N. Morimoto, and S. Ando, "Tactile sensing using tensor cell," in *Proc. IEEE Int. Conf. Robotics and Automation*, 1995, pp. 825–830.

[13] M. R. Shah, R. P. Phillips, and R. A. Normann, "A study of printed spiral coils for neuroprosthetic transcranial telemetry applications," *IEEE Trans. Biomed. Eng.*, vol. 45, pp. 867–876, July 1998.

[14] M. Hakozaki, K. Nakamura, and H. Shindoa, "Telemetric artificial skin for soft robot," in *Proc. TRANSDUCERS'99*, 1999, pp. 1042–1045.

[15] T. Maeno, T. Kawai, and K. Kobayashi, "Analysis and design of a tactile sensor detecting strain distribution inside an elastic finger," in *Proc. IEEE/RSJ Int. Conf. Intelligent Robots and Systems*, 1998, pp. 1658–1663.

[16] H. Shinoda, S. Sasaki, and K. Nakamura, "Instantaneous evaluation of friction based on ARTC tactile sensor," in *Proc. IEEE Int. Conf. Robotics and Automation*, 2000, pp. 2173–2178.


**Hiroyuki Shinoda** received the B.S. degree in applied physics, the M.S. degree in information physics, and the Ph.D. degree in electrical engineering from the University of Tokyo, Tokyo, Japan, in 1988, 1990, and 1995, respectively.

He is currently an Associate Professor in the Department of Electrical and Electronic Engineering, Tokyo University of Agriculture and Technology, Tokyo, Japan. His current research focuses on sensor systems and devices, including tactile sensors and optical/acoustic biosensors based on MEMS technologies, haptic interfaces in VR, including a realistic tactile feeling display, and a nonvibratory ultrasonic device for new ultrasound applications.

Prof. Shinoda received the Best Conference Paper Award at IEEE ICRA'99.

**Hideki Oasa** received the B.S. degree in electronic and information engineering in 1998 from Tokyo University of Agriculture and Technology, Tokyo, Japan, where he is currently a graduate student in the Department of Electrical and Electronic Engineering.

His research interests are signal processing and devices for tactile sensing.